Continental Shelf Research 30 (2010) 752–760

Contents lists available at ScienceDirect

Continental Shelf Research

journal homepage: www.elsevier.com/locate/csr

Spatial and temporal variability of satellite-derived sea surface temperature in the southwestern Atlantic Ocean

Andrés L. Rivas *

Centro Nacional Patagónico (CENPAT-CONICET), Boulevard Brown s/n, (9120) Puerto Madryn, Chubut, Argentina

ARTICLE INFO

Article history:
Received 21 May 2009
Received in revised form
23 December 2009
Accepted 13 January 2010
Available online 20 January 2010

Keywords:
Southwest Atlantic Ocean
Sea surface temperature
Seasonal variability
Interannual variability
Long-term temperature trend

ABSTRACT

Mean fields, seasonal cycle, and interannual variability of the Southwestern Atlantic Ocean (SAO) sea surface temperature (SST) distribution are examined during an 18-year (January 1985–December 2002) period by means of monthly composite, around 9 km resolution satellite-derived SST data. Temporal evolution of the mean spatial value shows a very marked annual cycle, certain interannual variability and a weak increasing tendency (~0.06 °C/decade). Spatial distribution of the mean temporal value shows the influence of the horizontal advection over the SST field. Over 90% of the temporal variability is explained by the annual harmonic, which reaches amplitudes of 7 °C over the shallowest zones. The inclusion of the semiannual harmonic improves the description of the seasonal cycle only in those regions of the domain where warming and cooling cycles show different durations. The strong correlation between the surface heat flux and the SST allows, by means of a single diffusion equation, the prediction of the shelf areas which do not stratify seasonally. The EOF analysis shows three modes (which together explain over 97% of the variance) associated with the stationary value, the amplitude and the phase of the annual harmonic, i.e., with the seasonal cycle. The fourth mode (0.22% of the variance) is the first one to show interannual variability, which is well correlated with the Southern Annular Mode (SAM).

1. Introduction

Seasonal sea surface temperature (SST) variability and the physical processes associated to it are of great importance in ecosystem regulation. Long period interannual variability plays a fundamental role in climatic studies. Additionally for over 20 years satellite sensors have provided, quasi-synoptic and high time-space resolution information on the SST over an area that has been historically undersampled by conventional methods.

The seasonal cycle in the Southwestern Atlantic Ocean (SAO) accounts for over 90% of the variance (Podestá et al., 1991; Provost et al., 1992; Rivas, 1994; Lentini et al., 2000) and also regulates algal blooms and different species migrations. Vertical stratification conditions CO_2 exchange with the atmosphere and its regional balance (Bianchi et al., 2005 and 2009). North of Río de la Plata, Campos et al. (1999) and Lentini et al. (2000) suggested certain coupling between SST anomalies propagation and El Niño Southern Oscillation (ENSO), while other authors have correlated these anomalies to precipitation (Hasternrath and Greischar, 1993a,b; Carton et al., 1996; Diaz et al., 1998; Camilloni and Barros, 2000). More recently, Barrucand et al. (2008) showed that the frequency of warm events (especially warm nights) is highly associated with the SST in coastal zones and that the main variability mode found was an 8-year wave signal noticeable in the analysis of cold nights, Atlantic SST and the Southern Annular Mode (SAM).

The study area (Fig. 1) covers two different hydrographic regimes. The continental shelf is wide (at 50°S it reaches almost 900 km of extension), with high tide amplitudes (over 12 m in the south zone) and shows a mean north–northeastward surface flow (Palma et al., 2008). In winter, the water column along the shelf becomes vertically homogeneous because of the direct wind mixing and the vertical convection associated with the loss of buoyancy of the surface waters. Between the end of spring and the beginning of fall, the water column over the shelf stratifies, except for those zones where tide mixing is enough to balance the effect of the surface heat flux, giving rise to various thermal fronts which have strong influence on phytoplankton blooms (Rivas, 2006). In the oceanic zone the Brazil Current (BC) flows southwards along the continental slope carrying subtropical warm and salty water as part of the South-Atlantic anticyclonic gyre. Malvinas (also known as Falkland) Current (MC) is a detachment of the Antarctic Circumpolar Current (ACC) that flows northward carrying cold water (Piola and Gordon, 1989). At approximately 38°S these two currents meet and generate a quasi-stationary meander that extends up to approximately 45°S. Olson et al. (1988); Garzoli and Garraffo (1989); Chelton et al.

* Fax: +54 2965 451543.
E-mail address: andres@cenpat.edu.ar

0278-4343/$ - see front matter © 2010 Elsevier Ltd. All rights reserved.
doi:10.1016/j.csr.2010.01.009

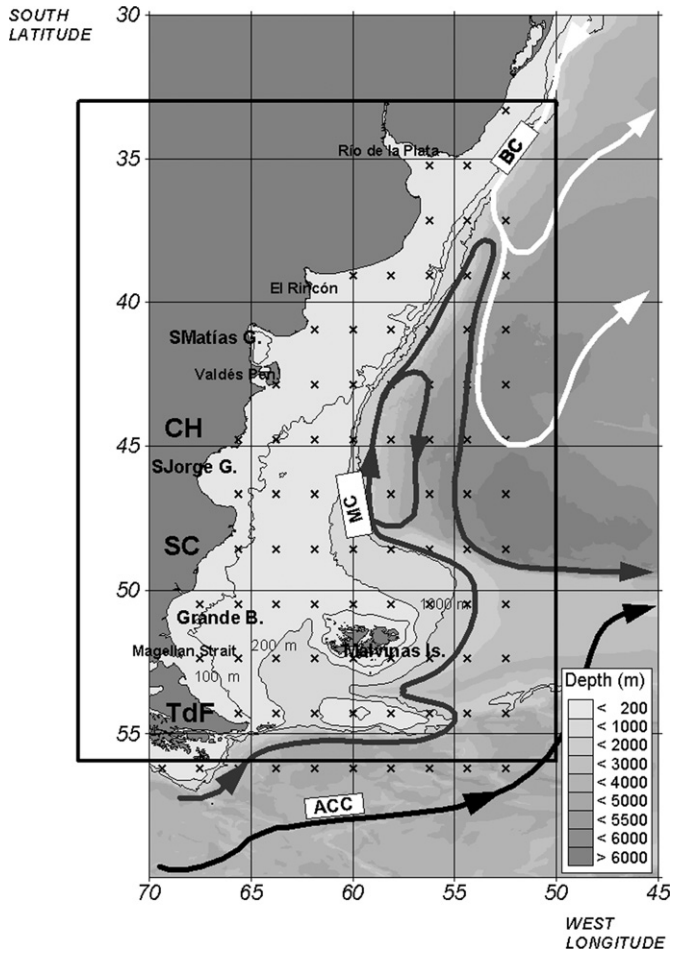

Fig. 1. Schematic circulation of Southwestern Atlantic Ocean (SAO), showing the Malvinas (also known as Falkland) (MC), Antarctic Circumpolar (ACC) and Brazil Currents (BC) (adapted from Piola and Rivas, 1997). Shown in grey tones is the bathymetry and in black lines the 100, 200 and 1000 m isobaths. Inside the black line rectangle is the study area and major geographic features. Abbreviations are: **CH** Chubut, **SC** Santa Cruz and **TdF** Tierra del Fuego provinces. The location of NCEP nodes with surface heat flux data is indicated by the X points.

(1990) and Piola and Matano (2001), among others, have described these currents and their zone of influence.

The objective of this study is to provide a detailed description of the time and spatial evolution of the SST in the SAO (Fig. 1), using an 18-year (1985–2002) series of monthly composite satellite images.

2. Data

Eighteen years of SST data (from January 1985 to December 2002) obtained by the Advanced Very High-Resolution Radiometer (AVHRR) on board of NOAA satellites, processed by the Pathfinder project version 4.1 and available at http://poet.jpl.nasa.gov were used for this study. These data consist of monthly composite images with a resolution of $\sim$9 km, which cover an area in the Southwestern Atlantic defined by parallels 33 and 56°S, the 55°W meridian and the coast. The number of valid SST retrievals for each of the 39796 grid points employed ranged between 176 and 216.

Heat fluxes were taken from the National Center for Environmental Prediction-National Center for Atmospheric Research (NCEP-NCAR) reanalysis (Kalnay et al., 1996) dataset. Monthly averaged data are provided on a grid with a resolution of approximately $2^\circ \times 2^\circ$ in 85 points over the study area (Fig. 1).

The circulation variability of the lower atmosphere in the southern hemisphere is dominated by an annular mode that significantly influences the strength of the westerlies. This mode has been referred to as the Southern Annular Mode (SAM) and defined as the leading principal component of the 850 hPa geopotential height anomalies south of 20°S (Thompson and Wallace, 2000). The SAM index time series can be found at http://www.cpc.noaa.gov. A positive (negative) SAM index is associated with lower (higher) sea level pressures at high latitudes and higher (lower) sea level pressures at low latitudes. As a consequence, during years with a positive SAM index, the westerlies are intensified in the Antarctic Circumpolar Current (ACC) region and weakened north of 40°S.

3. Results and discussion

This section presents the spatial and temporal averages, harmonic analyses of SST and a decomposition of SST with empirical orthogonal functions (EOFs).

3.1. Mean spatial value

The mean value over the whole domain is giving by:

$$< \mathrm{T}(t_i) > = 1/N \Sigma_j T(x_j,\ t_i)$$

where N=39796 is the number of data points. Spatial mean shows a well-defined annual cycle (Fig. 2a) and certain interannual variability, while there is not a very marked long period tendency (lower than +0.06 °C decade^{-1}). The surface heat flux averaged over the whole domain (85 NCEP nodes) shows similar characteristics (Fig. 2b). In this case, the long period tendency is also very small but decreasing (less than -4 W m^{-2} decade^{-1}). The correlation between these series is maximum (0.93) for a lag of two months. The standard deviations (s.d.) of the mean spatial values show opposite behaviors. SST is spatially more homogeneous during the cold period, when the mixed layer is deeper and more uniform over the whole domain (Fig. 2a). The surface heat flux shows higher spatial variability when solar radiation is minimum, the net heat flux is from the sea to the atmosphere and basically regulated by the air–sea interface (Fig. 2b).

The variability is computed by removing the mean seasonal cycle, calculated at every grid point. Departures from the seasonal cycle are defined as "anomalies". Afterwards, mean spatial anomalies are calculated by averaging the anomalies from all the pixels with available information (Fig. 2c). Mean surface heat flux anomalies were estimated in the same way (Fig. 2d). Correlation between the two series resulted insignificant (0.11) at the 95% significance level (0.13).

Regardless of the spatial variability, i.e., analyzing mean spatial values, SST field shows a very marked annual cycle, which is attributable to the surface heat flux. On the contrary, deviations from this seasonal cycle are not correlated with the deviations of the surface heat flux from its seasonal cycle. Long-term tendencies do not show correlation either. While the SST shows an increasing tendency, the surface flux shows a decreasing tendency.

Recent analysis of satellite images (Gregg et al., 2005; Saraceno et al., 2005; Rivas et al., 2006) detected higher surface chlorophyll levels during the last few years, which could be associated to a decrease in the SST accompanied with a higher inflow of nutrients into the photic zone. This decreasing tendency of the SST is not evident among the analyzed data. The reason for this discrepancy could be that the zone where satellite chlorophyll rises more evidently circumscribes to the continental shelf, while this analysis includes also the oceanic zone, or else, due to the difference in temporal extension of the satellite SST and sea color data.

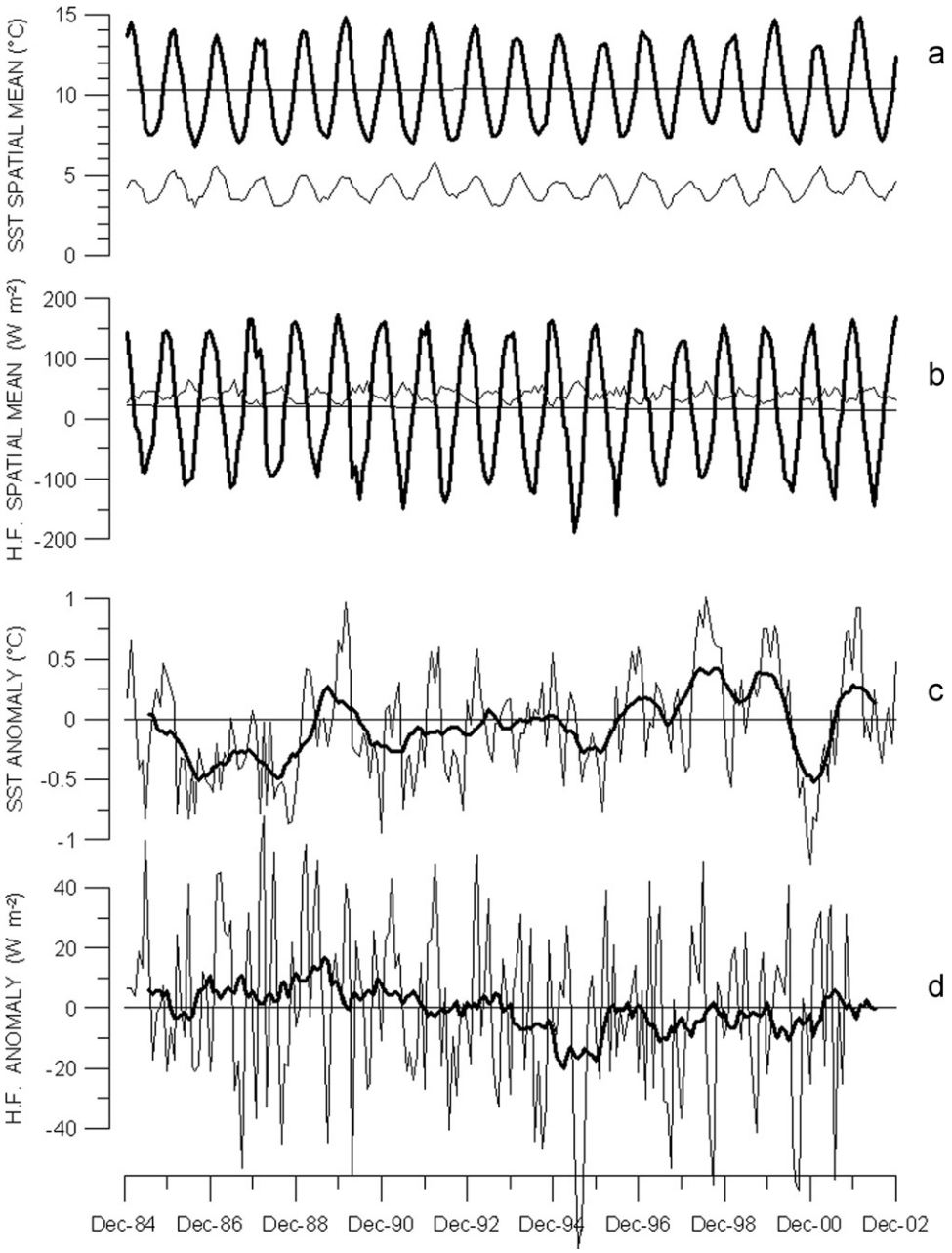

Fig. 2. Temporal evolution of the spatial average of the monthly values (thick line), long period tendency (straight line) and its corresponding standard deviation (thin line) for the SST (**a**), and the surface heat flux (**b**). Monthly mean values of the spatial anomaly with respect to the climatological annual cycle (thin line) and series smoothed with a 1 yr running mean filter (thick line) for the SST (**c**), and the surface heat flux(**d**).

Belkin (2009) recently has calculated an increasing tendency of 0.032 °C decade^{-1} in the Large Marine Ecosystems of Patagonian Shelf in the period 1982–2006. Considering that neither the analyzed zones nor periods analyzed agree exactly, it is possible to affirm that their results are coherent with the present work.

3.2. Mean temporal value

The average of the 216 values registered monthly at each point

$$T_0(x_j) = 1/216 \Sigma_i T(x_j,\ t_i),$$

shows (Fig. 3a) the influence that water dynamics have on the spatial distribution of SST. The Argentine Basin shows the effects of the BC, the MC and its retroflexion and, to a lesser extent, the effect of the ACC. Over the continental shelf it is possible to distinguish the influence of the input of cold water through the Magellan Strait, coastal regions with lower mean SST due to the absence of seasonal vertical stratification (for example, the coastal region South of San Jorge Gulf and the one close to Peninsula Valdés) as well as regions more isolated from the general north–northeastward flow, where mean SST is higher since it is less exposed to the southerly cold water advection (for example, inside San Matías Gulf or near El Rincón). Variability associated to the mean temporal value, given by its s.d. (Fig. 3b), is mostly due to the annual signal, as it will be shown later.

3.3. Annual cycle

The stationary signal as well as the annual and semiannual harmonics for each pixel with more than 180 valid data were

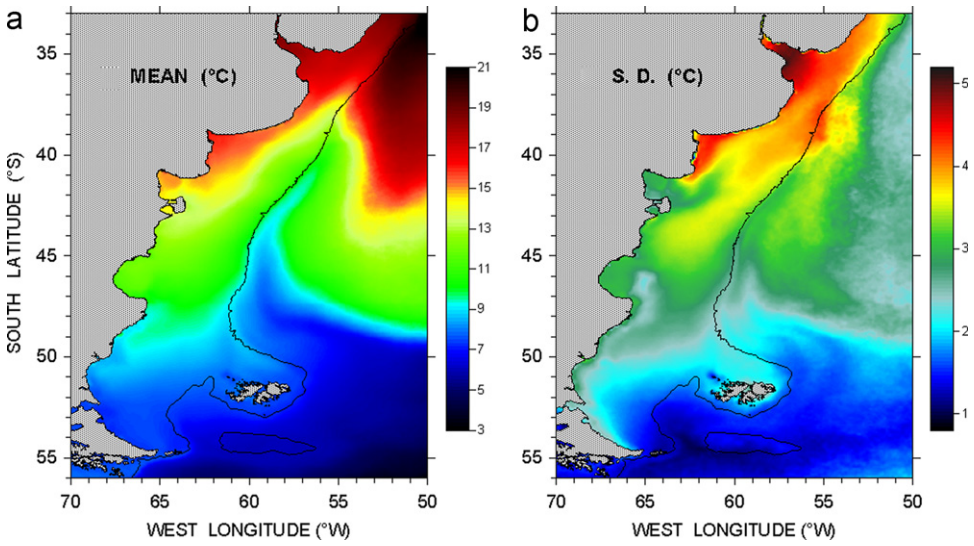

Fig. 3. Spatial distribution of the temporal mean SST (**a**), and its corresponding standard deviation (**b**).

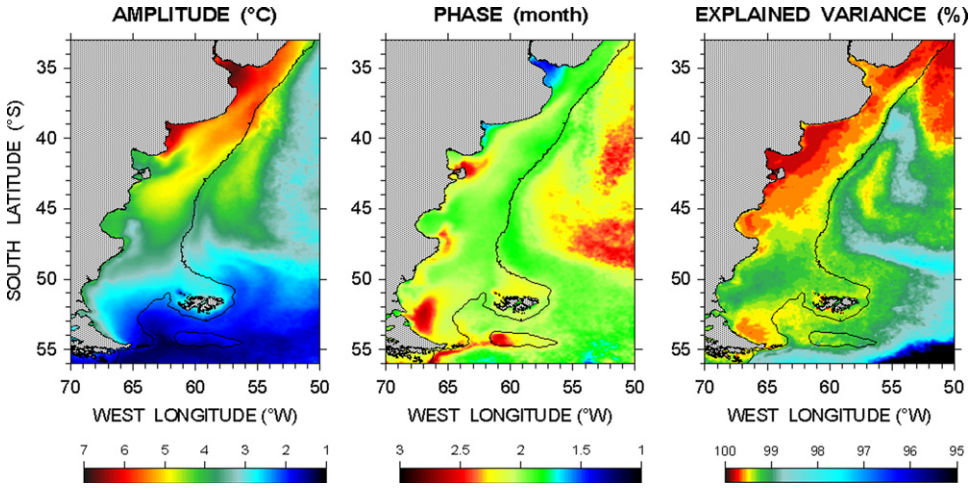

Fig. 4. Spatial distribution of the amplitude (°C), the phase (months) and the percentage of explained variance for the annual harmonic.

calculated using a least square adjustment. (Beron-Vera and Ripa, 2000). Fig. 4 shows the amplitude, the phase and the percentage of the explained variance by the annual harmonic. The preponderance of the annual signal, evidenced by the percentage of explained variance, has a simple physical interpretation, since the surface heat flux is also dominated by this frequency. The amplitude of the annual signal shows a spatial structure similar to the s.d. of the mean temporal value (compare Figs. 4a and 3b), demonstrating that, at each point, temporal variability is mostly due to the annual cycle. The amplitude of the annual harmonic over the shelf usually rises towards the North, reaching maximum values (between 6 and 7 °C) at the very shallow coastal zones (less than 40 m depth) of El Rincón and Río de la Plata. In general, the annual cycle amplitude is lower in zones that do not stratify seasonally, where summer heat flux is distributed over the whole water column. Zones where turbulent mixing giving by tides (Glorioso and Flather, 1995; Palma et al., 2004) keeps the water column homogeneous even in summer, were identified near Valdés Peninsula, the north coast of Santa Cruz and the north–west of Malvinas islands. Krepper and Rivas (1979) and Sabatini et al. (2004) have shown the absence of vertical stratification south of 51°S. Besides that, is recognized the strong vertical mixing (barotropic nature) of the MC flow.

Regardless of the semiannual component, the fit reduces to:

$$T(x,\ t) = T_0(x) + T_1(x)\cos[\omega(t - t_o)],$$

and in this case, the annual harmonic phase t_o (Fig. 4b) indicates the moment of the year with maximum SST. It can be seen that the SST over the shelf reaches its maximum between February 1 (phase=1.5 months) and March 1 (phase=2.5 months), and that it is lower in the shallow zones of Río de la Plata and El Rincón, and higher in those zones that remain homogeneous over the year (near of Valdés Peninsula, south end of San Jorge gulf, coast of Tierra del Fuego and a small area located NW of Malvinas islands).

Amplitude distributions and the phase of the signal both coincide with the results obtained by Podestá et al. (1991) using data with lower spatial resolution ($1^\circ \times 1^\circ$ vs. 9×9 km), shorter record length (4 years vs. 18 years) and higher temporal resolution (5 days vs. 1 month).

Regarding the explained variance by the annual harmonic, Fig. 4c shows that over the shelf it is always higher than 98%. Considering the whole domain, the lowest values of the explained variance are located at the confluence of BC and MC, and at the region between the main MC flow and its return. It is possible that this decrease is caused by mesoscale processes that are seen over these regions even using monthly averaged data. When

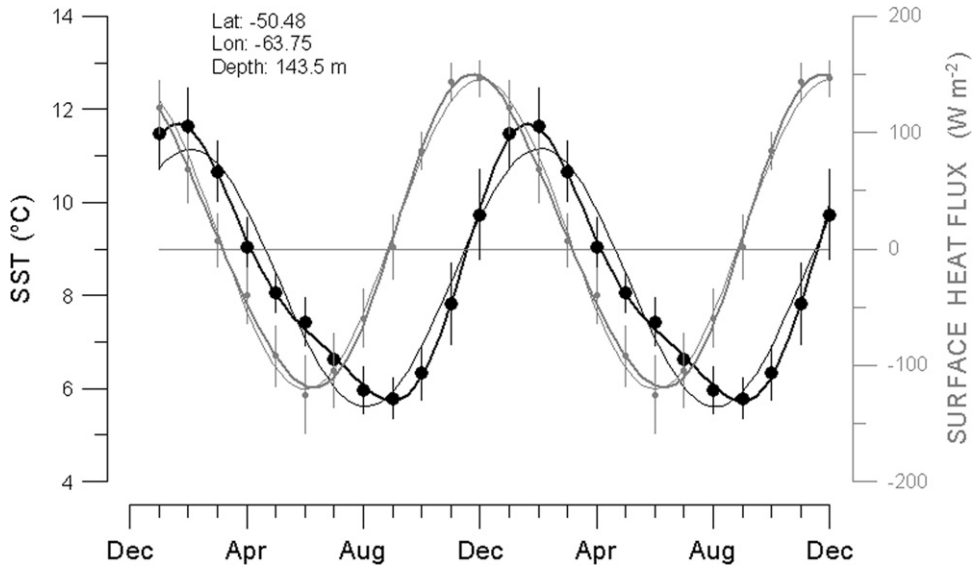

Fig. 5. Observed values (dots), their corresponding standard deviations (bars), fit only to the annual harmonic (thin line) and fit to the annual and semiannual harmonics (thick line) of the climatological SST seasonal cycle (black) and the surface heat flux (grey), at the indicated grid point.

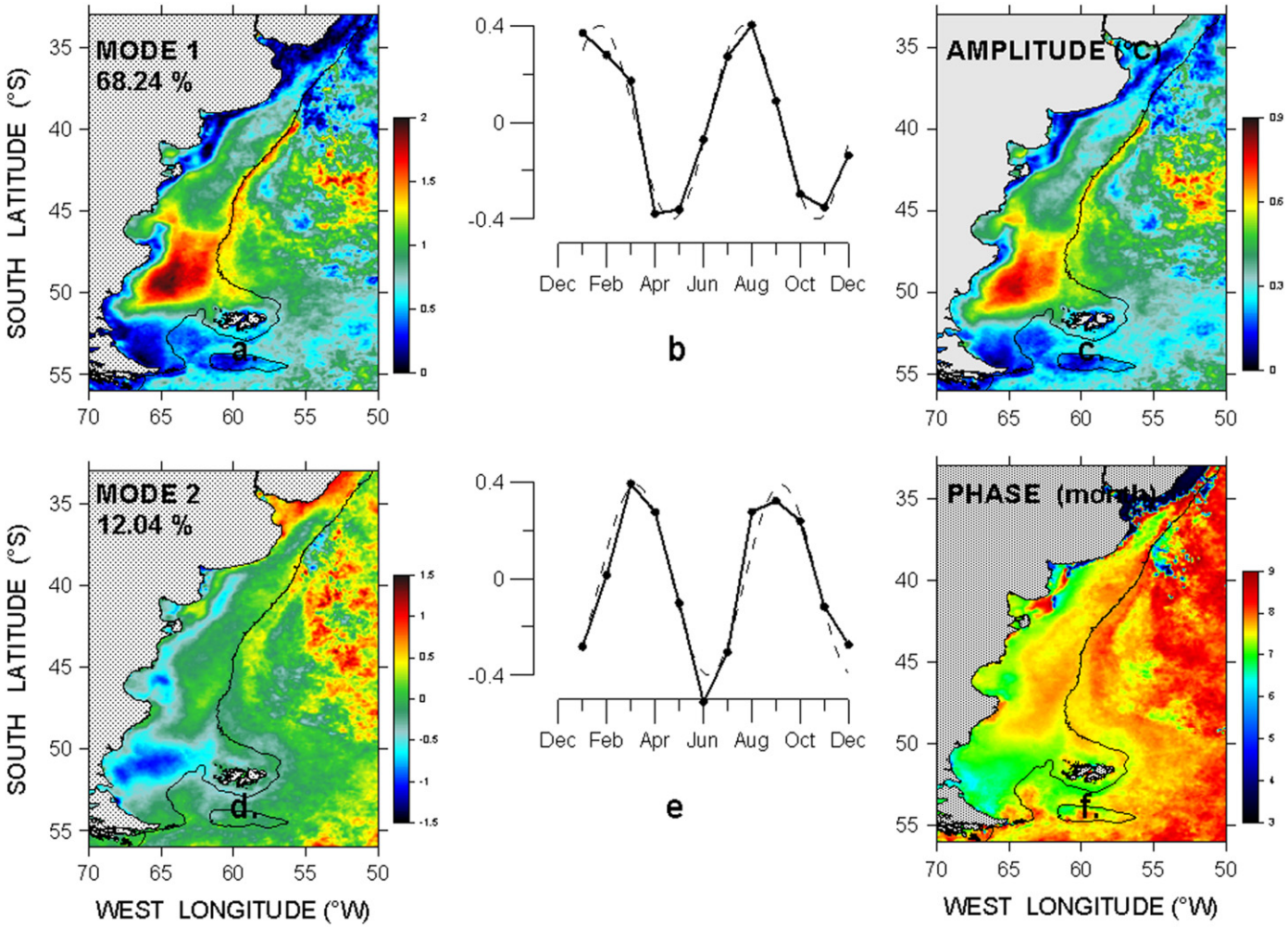

Fig. 6. First and second spatial (**a** and **d**) and temporal (**b** and **e**) modes of the EOFs decomposition of the climatological anomalies (climatological seasonal cycle minus the annual harmonic fit). In **b** and **e,** a dotted line showing the fit to a semiannual signal is included. Spatial distribution of the amplitude (**c**) and the phase (**f**) for the semiannual harmonic.

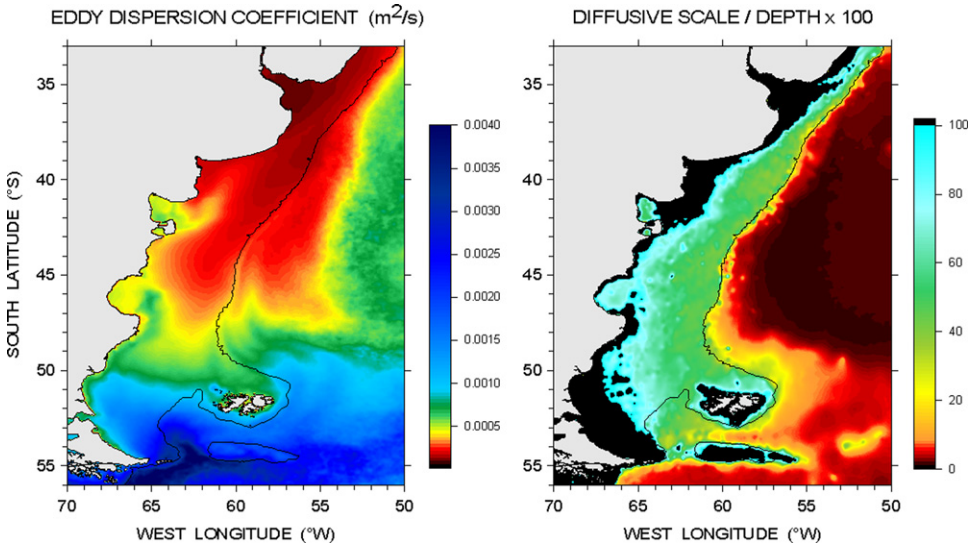

Fig. 7. Vertical turbulent diffusion coefficients estimated from the model ($m^2\,s^{-1}$) and vertical diffusion scale (see text for its definition) drawn as percentage of the local depth. The zones where the diffusive scale exceeds the local depth indicate the absence of vertical stratification.

interpreting the high values of variance explained by the annual adjustment, it has to be considered that due to the resolution of the data used, variability associated to scales below one month and 9 km is filtered. Additionally, the residuals from the fit are assumed as statistically independent or uncorrelated which is often inappropriate for geophysical time series. In this case, the effective number of independent realizations (effective degrees of freedom) could be less than the total number of sample observations and the proportion of variance explained by the regression (the r^2 coefficient) would be overestimated.

The semiannual harmonic only explains, in average, less than 0.1% of the variability (it does not get to explain 1% of the original variance of the data at any point of the domain). The amplitudes of the semiannual harmonic are one order of magnitude below those of the annual harmonic. When including the semiannual harmonic, the average difference between maximum and minimum temperatures varied less than 1% (at no point of the domain this change is greater than 13%), i.e. the semiannual signal does not change the seasonal cycle amplitude. The annual harmonic predicts 6 months of heating and 6 months of cooling, the inclusion of the semiannual harmonic breaks this symmetry. It can be seen that in those zones where the amplitude of the semiannual harmonic is higher, the heating period shortens. The asymmetry between the heating and the cooling cycles had already been documented for the shelf zone by Krepper and Bianchi (1982). The maximum SST is reached prematurely when the surface heat flux is still from the atmosphere to the sea, and the minimum surface temperature is reached over 6 months later, when the surface heat flux is again from the atmosphere towards the sea. The advection of cold water in the N–NE direction, besides balance the annual surface net heat flux (which is positive over practically the whole domain) is probably responsible for the early beginning of the cooling period, which could last up to 7.5 months. Fig. 5 shows this situation for a point located at 63.75°W, 50.48°S. Even when the explained variability and the amplitude of the seasonal cycle do not change significantly, this figure shows that the adjustment to the data with the full signal (annual and semiannual) is better than the one obtained using only the annual signal.

The annual climatological cycle was calculated at each pixel, averaging for each month the SST over the 18 years, and afterwards the monthly mean anomalies were calculated by subtracting the annual harmonic estimated in each point of the domain.

These 12 series with 39,796 points each were decomposed into empirical orthogonal functions (EOFs), obtaining two modes which together explain over 80% of the variance. The first of these two modes (68.24% of the explained variance) shows a spatial structure (Fig. 6a) very similar to the distribution of the semiannual harmonic amplitude (Fig. 6c), while the corresponding eigenvalue exhibits a clear semiannual cycle (Fig. 6b). The second mode (12.04%) shows a spatial structure (Fig. 6d) similar to that calculated for the phase of the semiannual harmonic (Fig. 6f) and its eigenvalue also shows a very marked semiannual signal (Fig. 6e).

From this analysis it can be concluded that the climatological annual cycle is fundamentally explained by the annual harmonic which predicts the seasonal amplitude almost exactly and that the semiannual harmonic, by allowing the asymmetry between the heating and cooling periods, give a more detailed description.

3.4. *Vertical structure—model*

Not considering the horizontal heat fluxes, disregarding the vertical advection and assuming a constant vertical diffusion coefficient (in time and along the whole water column), the heat conservation equation is reduced to a vertical diffusion equation:

$$\partial_t T(z,\ t) = K\partial_{zz} T(z,\ t)$$

For simplicity, the temperature T is considered to be forced only by the annual component of the surface heat flux, then the boundary condition is:

$$K\rho C_p \partial_z T(z,\ t) = F_1 \cos[\omega(t - t_f)],\ \text{ in } z = 0$$

where ρ is the density, C_p the heat capacity of sea water, F_1 is the amplitude of the annual component of the surface flux, t_f its phase and ω equals one cycle per year.

Omitting the boundary conditions that no heat passes through the sea bed ($z = -D$), the solution to this model is:

$$T(z,\ t) = \tau e^{z/H} \cos[\omega(t - tf) + z/H - \pi/4] \quad (1)$$

where $\tau = F_1\, H\, (K\rho\, Cp\, \sqrt{2})^{-1}$ and $H = (2K\,\omega^{-1})^{1/2}$ is a vertical diffusive scale. With a condition of zero heat flux at the bottom, the solution gets mathematically more complicated but it is not significantly different (see Prandle and Lane, 1995 or Smerdon and Stieglitz, 2006) and it is simple to identify the same diffusive scale.

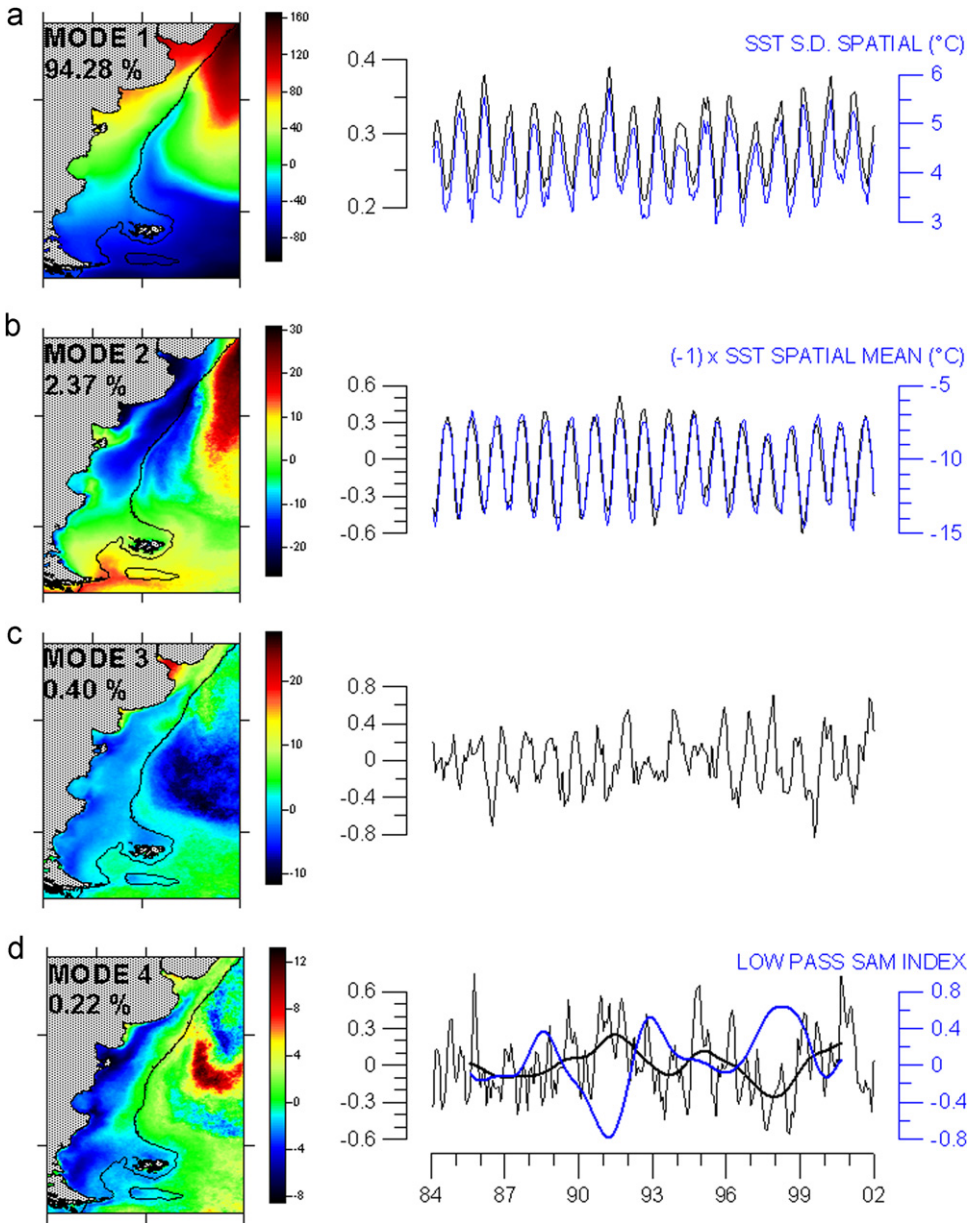

Fig. 8. First four modes of the EOFs decomposition. In the temporal mode 1 (**a**) the s.d. of the mean value has been included in blue. In the temporal mode 2 (**b**) the blue line indicates the mean spatial values. The temporal mode 4 (**d**) includes smoothed series with a mean filter that eliminates frequencies higher than the annual of this mode (thick black line) and those of the SAM index (blue line). (For interpretation of the references to color in this figure legend, the reader is referred to the web version of this article.)

The least squares fit to the SST data allowed the calculation of τ (the surface amplitude of the annual harmonic) at each point of the domain. $F1$ was calculated in the same way from the surface heat flux data at the 85 NCEP nodes. Afterwards $F1$ values were interpolated to all the points in the domain and diffusion coefficients K that satisfied the solution (1) were estimated. These K values were used to calculate the diffusive vertical scale H. Fig. 7 shows the values obtained for K and H, with H relative to the total depth D. The values of K obtained for the shelf ranges from $1–10 \times 10^{-4}\,m^2\,s^{-1}$ and are comparable to those derived by Malacic (1991) for describing the annual temperature cycle. In those places where $H \gg D$, the local depth, the solution obtained indicates that the annual harmonic of the temperature will have almost the same amplitude and phase from surface to bottom, i.e., the water column will be isothermal. Zones where H exceeds the depth D are shown in Fig. 7b and, considering those zones as indicative of the areas with no vertical stratification, the result agrees pretty acceptably with the estimations of the Simpson parameter calculated from hydrographic data (see Fig. 6 in Sabatini et al., 2004; Fig. 4 in Bianchi et al., 2005; Fig. 2 in Bogazzi et al., 2005 and Fig. 8 in Lucas et al., 2005). The major discrepancies appear in the zone of Río de la Plata where, even when the estimated K value is low, the vertical diffusive scale for the annual cycle exceeds the total depth D. In that region, water column stability is dominated by the discharge of fresh water.

These simple calculations show that the spatial distribution of the annual cycle amplitude over the shelf is partly ruled by the stratification conditions, and also that surface satellite observations can, under certain conditions, provide information on the vertical structure of the whole water column.

3.5. EOF decomposition

EOF analysis was applied to the data set normalized by subtracting the spatial average from each individual image and dividing it by the s.d.. The so-called gradient modes (Paden et al., 1991) were used to investigate the seasonal and interannual variability and respective spatial patterns. The first four modes were selected for physical interpretation since they contained a signal greater than the level of noise (Overland and Preisendorfer, 1982).

The first mode explains 94.28% of the variance and shows a spatial structure (Fig. 8a) similar to the mean temporal value (Fig. 3a). Its temporal mode shows a very marked annual signal and an evolution similar to the s.d. of the spatial mean (Fig. 2a). Even when it is spatially similar to the mean temporal value, this mode gives extra information because its temporal evolution shows that its spatial pattern intensifies in summer. The second mode explains 2.37% of the variance and its spatial structure (Fig. 8b) is similar to that of the annual harmonic amplitude (Fig. 4a). In time, it shows the prevalence of a very marked annual cycle with a temporal evolution similar to that shown by the mean spatial value (Fig. 2a) with opposite sign (i.e., high values in winter and low in summer). Spatially (Fig. 8c), the third mode (0.40% of the variance) is similar to the phase distribution of the annual harmonic (Fig. 4b) and temporally it shows the prevalence of an annual signal, though not so regular. These modes, which together explain over 97% of the variance, are associated to the mean temporal value, the amplitude and the phase of the annual harmonic, evidencing once more the importance of this signal. The fourth mode explains 0.22% of the original variance and 7.4% of the variance not explained by the first three modes. Even when the variance that explains this mode is marginal, it is included in the analysis for it is the first one to show a considerable interannual variability. Spatially it shows two domains. One at the continental shelf with negative values of greater magnitude over the zones that do not stratify seasonally, and the other one external, with positive values associated to the MC and its retroflection (Fig. 8d). Its temporal eigenvalue exhibits variability a frequencies higher than the annual one, and as it was mentioned before, it is the first to show an appreciable interannual signal. To highlight the interannual variability a low-pass filter that eliminates frequencies higher than one year was used (a running average of 13 elements and then two running averages of 12 elements each were applied successively, with a total of 34 lost data). The obtained series was correlated to its analogue for the SAM index. Correlation between both filtered series is -0.71 (the 99% significance level is 0.60). Using lower spatial resolution data it has already been shown (Lovenduski and Gruber, 2005 and Meredith et al., 2008) that the SAM index correlates positively with the SST over the southeast region of the domain and negatively over the north region. However, the spatial pattern of this correlation does not coincide with that of the analyzed mode. The SAM wind anomalies have both, a dynamic (e.g., via Ekman transport) and a thermodynamic effect on the ocean through surface stresses and by affecting heat and freshwater fluxes, respectively. The westerly wind intensification over the Drake Passage region (SAM >0, see Meredith et al., 2008) can be associated to a higher northward advection of cold water by the MC. The subsequent decrease in the SST over the MC influence zone enhance in its retroflection where probably a displacement of warmer water of subtropical origin occurs. North of 55°S a SAM >0 index generates a negative anomaly in both wind components (see Meredith et al., 2008) and with a less intense wind, it is reasonable to consider a positive SST anomaly over the shelf since the depth of the mixed layer decreases. However, this anomaly is more intense in coastal zones, vertically homogeneous due to the effect of tides, which indicates that there must be a change in the surface heat flux. This possibility was explored using NCEP data, but the spatial resolution of this information (approximately 2 degree) does not allow resolving the spatial scale of these frontal areas.

4. Summary and conclusions

In this paper high-resolution satellite-derived SST data were used to study spatial and temporal SST variability over a large domain in the SAO between 1985 and 2002. Determination of the spatial and temporal variability of SST from these highly productive regions using high-resolution, satellite-derived data may lead to a better understanding of the coupling between physical and biological oceanographic processes and of the interactions between the ocean and the atmosphere.

Findings from this study include:

a. The mean spatial value (which is equivalent to considering the temporal variability of the whole domain as it was a point) shows a very clear annual cycle, certain interannual variability and a slight increasing tendency in SST. This series shows a very good correlation with the one for the surface heat flux (0.93 with a two months delay), but neither the long-term tendencies nor the seasonal cycle anomalies show the same correspondence. The respective standard deviations show that while the SST is more homogeneous in winter, the heat flux is more uniform in summer.
b. The mean temporal value (which is equivalent to considering spatial variability of the stationary field) shows the influence of the circulation over the zones where horizontal advection is increased (MC, BC, ACC, etc.) as well as over those more isolated, where advection is diminished (El Rincón, San Matías gulf).
c. The SST shows a very marked seasonal cycle (mean difference between winter and summer on the order of 7 °C) explained basically by the annual harmonic. The distribution of the amplitudes and phases can be interpreted regarding each zone particularities. The inclusion of the semiannual harmonic only improves the cooling and heating period determination over some areas, but do not improve the seasonal cycle amplitude. This is interesting since, assuming that vertical stratification begins when the SST reaches its minimum, this moment would be indicating the beginning of fair conditions for the development of the spring bloom, a very important pattern of the surface chlorophyll distribution over the whole shelf (Rivas et al., 2006).
d. Using a simple model, the high resolution of the used data allowed inferring the areas that remain mixed during summer due to the tidal mixing. These results are very consistent with those obtained from historical and recent hydrographic data (temperature and salinity profiles obtained using CTD or bottles and reversing thermometers) showing the possibility of obtaining information on the vertical structure of the water column from satellite data. This result is also interesting for analyzing chlorophyll distribution patterns, since it reaches very high concentrations in frontal zones (Rivas, 2006).
e. The EOF decomposition, besides showing the almost exclusive contribution of the annual cycle in explaining the variance of the analyzed data, permitted to infer some of the interannual mechanisms of variability. This variability was correlated to the SAM index and interpreted based on its dynamic effects. Describing the spatial pattern using appropriate resolution data led to the identification of a differential behavior between shelf waters and those influenced by de MC, something not

shown by other works that use more widely spaced data. Interannual variability over the shelf zone is probably more influenced by thermodynamic effects related to SAM, but their identification was not possible considering the low resolution of available atmospheric information.

Acknowledgments

SST data were obtained from NASA Physical Oceanography Distributed Active Archive Center at the Jet Propulsion Laboratory. We also thank N. Glembocki for language corrections. This research was partially supported by Fundación Antorchas grant No. 13900-13.

References

Barrucand, M., Rusticucci, M., Vargas, W., 2008. Temperature extremes in the south of South America in relation to Atlantic Ocean surface temperature and Southern Hemisphere circulation. Journal of Geophysical Research 113, D20111, doi:10.1029/2007JD009026.

Belkin, I.M., 2009. Rapid warming of large marine ecosystems. Progress in Oceanography, 81 (1–4), 207–213, doi:10.1016/j.pocean.2009.04.011.

Beron-Vera, F.J., Ripa, P., 2000. Three-dimensional aspect of the seasonal heat balance in the Gulf of California. Journal of Geophysical Research 105 (C5), 11441–11457.

Bianchi, A.A., Bianucci, L., Piola, A.R., Ruiz Pino, D.I., Schloss, I., Poisson, A., Balestrini, C.F., 2005. Vertical stratification and air-sea CO_2 fluxes in the Patagonian shelf. Journal of Geophysical Research 110, C07003, doi:10.1029/2004JC002488.

Bianchi, A.A., Ruiz Pino, D., Isbert Perlender, H.G., Osiroff, A.P., Segura, V., Lutz, V., Luz Clara, M., Balestrini, C.F., Piola, A.R., 2009. Annual balance and seasonal variability of sea-air CO_2 fluxes in the Patagonia Sea: Their relationship with fronts and chlorophyll distribution. Journal of Geophysical Research 114, C03018, doi:10.1029/2008JC004854.

Bogazzi, E., Baldoni, A., Rivas, A.L., Martos, P., Reta, R., Orensanz, J.M., Lasta, M., Dell'Arciprete, P., Werner, F., 2005. Spatial correspondence between areas of concentration of Patagonian scallop (Zygochlamys patagonica) and frontal systems in the southwestern Atlantic. Fisheries Oceanography 14 (3), 1–18.

Camilloni, I., Barros, V., 2000. The Parana River response to El Niño 1982–83 and 1997–98 events. Journal of Hydrometeorology 1, 412–430.

Campos, E.J.D., Lentini, C.D., Miller, J.L., Piola, A.R., 1999. Interannual variability of the sea surface temperature in the South Brazil Bight. Geophysical Research Letters 26 (14), 2061–2064.

Carton, J.A., Cao, X., Giese, B.S., da Silva, A.M., 1996. Decadal and interannual SST variability in the tropical Atlantic Ocean. Journal of Physical Oceanography 26, 1165–1175.

Chelton, D.B., Schlax, M.G., Witter, D.L., Richman, J.G., 1990. GEOSAT altimeter observations of the surface circulation of the Southern Ocean. Journal of Geophysical Research 95, 17,877–17,903.

Garzoli, S., Garraffo, Z., 1989. Transports, frontal motions and eddies at the Brazil Malvinas Currents Confluence. Deep Sea Research 36 (5), 681–703.

Diaz, A.F., Studzinski, C.D., Mechoso, C.R., 1998. Relationships between precipitation anomalies in Uruguay and southern Brazil and sea surface temperature in the Pacific and Atlantic oceans. Journal of Climate 11, 251–271.

Glorioso, P.D., Flather, R.A., 1995. A barotropic model of the currents off SE South America. Journal of Geophysical Research 100, 13427–13440.

Gregg, W.W., Casey, N.W., McClain, C.R., 2005. Recent trends in ocean chlorophyll. Geophysical Research Letters 32, L03606, doi:10.1029/2004GL021808.

Hasternrath, S., Greischar, L., 1993a. Further work on the prediction of Brazil rainfall anomalies. Journal of Climate 6, 734–758.

Hasternrath, S., Greischar, L., 1993b. Circulation mechanisms related to northeast Brazil rainfall anomalies. Journal of Geophysical Research 98, 5093–5102.

Kalnay, E., Kanamitsu, M., Kistler, R., Collins, W., Deaven, D., Gandin, L., Iredell, M., Sha, S., White, G., Woollen, J., Zhu, Y., Chelliah, M., Ebisuzaki, W., Higgins, W., Janowiak, J., Mo, K.C., Ropelewski, C., Wang, J., Leetmaa, A., Reynolds, R., Jenne, R., Joseph, D., 1996. The NCEP/NCAR 40-year Reanalysis Project. Bulletin of the American Meteorological Society 77 (3), 437–471.

Krepper, C.M., Bianchi, A.A., 1982. Balance calórico del Mar Epicontinental Argentino. Acta Oceanographica Argentina 3 (1), 119–133.

Krepper, C.M., Rivas, A.L., 1979. Análisis de las características oceanográficas de la zona austral de la Plataforma Continental Argentina y aguas adyacentes. Acta Oceanographica Argentina 2 (2), 55–82.

Lentini, C.A.D., Campos, E.J.D., Podestá, G.P., 2000. The annual cycle of satellite derived sea surface temperature on the western South Atlantic shelf. Brazilian Journal of Oceanography 48 (2), 93–105.

Lovenduski, N.S., Gruber, N., 2005. Impact of the Southern Annular Mode on Southern Ocean circulation and biology. Journal of Research Letters 32, L11,603, doi:10.1029/2005GL022727.

Lucas, A.J., Guerrero, R.A., Mianzán, H.W., Acha, E.M., Lasta, C.A., 2005. Coastal oceanographic regimes of the Northern Argentine Continental Shelf (34–43°S). Estuarine, Coastal and Shelf Science 65 (3), 405–420.

Malacic, V., 1991. Estimation of the vertical eddy diffusion coefficient of heat in the Gulf of Trieste. Oceanologica Acta 14 (l), 23–32.

Meredith, M.P., Murphy, E.J., Hawker, E.J., King, J.C., Wallace, M.I., 2008. On the interannual variability of ocean temperatures around South Georgia, Southern Ocean: Forcing by El Niño/Southern Oscillation and the Southern Annular Mode. Deep Sea Research Part II: Topical Studies in Oceanography 55 (18–19), 2007–2022.

Olson, D.B., Podestá, G.P., Evans, R.H., Brown, O.B., 1988. Temporal variations in the separation of Brazil and Malvinas currents. Deep Sea Research 35 (12), 1971–1990.

Overland, J.E., Preisendorfer, R.W., 1982. A significance test for principal components applied to a cyclone climatology. Monthly Weather Review 110, 1–4.

Paden, C.A., Abbott, M.R., Winant, C.D., 1991. Tidal and atmospheric forcing of the upper ocean in the Gulf of California, 1. Sea surface temperature variability. Journal of Geophysical Research 96 (C10), 18,337–18,359.

Palma, E.D., Matano, R.P., Piola, A.R., 2004. A numerical study of the South Western Atlantic Shelf circulation: barotropic response to tidal and wind forcing. Journal of Geophysical Research 109, C08014, doi:10.1029/2004JC002315.

Palma, E.D., Matano, R.P., Piola, A.R., 2008. A numerical study of the Southwestern Atlantic Shelf circulation: Stratified ocean response to local and offshore forcing. Journal of Geophysical Research 113, C11010, doi:10.1029/2007JC004720.

Piola, A.R., Gordon, A.L., 1989. Intermediate waters of the western South Atlantic. Deep Sea Research 36, 1–16.

Piola, A.R., Matano, R.P., 2001. Brazil and Falklands (Malvinas) Currents. In: Steele, J.H., Thorpe, S.A., Turekian, K.K. (Eds.), Encyclopedia of Ocean Sciences. vol. 1, pp. 340–349.

Piola, A.R., Rivas, A.L., 1997. Corrientes en la Plataforma Continental. In: El Mar Argentino y sus recursos pesqueros, TOMO 1: Antecedentes históricos de las exploraciones en el mar y las características ambientales (Edited by E.E. Boschi). Inst. Nac. Investigaciones y Desarrollo Pesquero (INIDEP), Mar del Plata, Argentina, 223 pp.

Podestá, G.P., Brown, O.B., Evans, R.H., 1991. The annual cycle of satellite-derived sea surface temperature in the southwestern Atlantic Ocean. Journal of Climate 4, 457–467.

Prandle, D., Lane, A., 1995. The annual temperature cycle in shelf seas. Continental Shelf Research 15 (6), 681–704.

Provost, C., Garcia, O., Garçon, V., 1992. Analysis of satellite sea surface temperature time series in the Brazil-Malvinas Current Confluence region: Dominance of the annual and semiannual periods. Journal of Geophysical Research 97 (C11), 17,841–17,858.

Rivas, A.L., 1994. Spatial variation of the annual cycle of temperature in the Patagonian shelf between 40 and 50° of south latitude. Continental Shelf Research 14 (13/14), 1539–1554.

Rivas, A.L., 2006. Quantitative estimation of the influence of surface thermal fronts over chlorophyll concentration at the Patagonian shelf. Journal of Marine Systems 63, 183–190, doi:10.1016/j.jmarsys.2006.07.002.

Rivas, A.L., Dogliotti, A.I., Gagliardini, D.A., 2006. Satellite-measured surface chlorophyll variability in the Patagonian shelf. Continental Shelf Research 26, 703–720, doi:10.1016/j.csr.2006.01.013.

Sabatini, M., Reta, R., Matano, R.P., 2004. Circulation and zooplankton biomass distribution over the southern Patagonian shelf during late summer. Continental Shelf Research 24, 1359–1373.

Saraceno, M., Provost, C., Piola, A.R., 2005. On the relationship between satellite retrieved surface temperature fronts and chlorophyll-a in the western South Atlantic. Journal of Geophysical Research 110, C11016, doi:10.1029/2004JC002736.

Smerdon, J.E., Stieglitz, M., 2006. Simulating heat transport of harmonic temperature signals in the Earth's shallow subsurface: Lower-boundary sensitivities. Geophysical Research Letters 33, L14402, doi:10.1029/2006gl026816.

Thompson, D.W.J., Wallace, J.M., 2000. Annular modes in the extratropical circulation. Part I: Month-to-month variability. Journal of Climate 13, 1000–1016.